Eur. Phys. J. B **26**, 493–502 (2002)
DOI: 10.1140/epjb/e20020118

THE EUROPEAN PHYSICAL JOURNAL B
EDP Sciences

Characteristics of transmission of electrons in a quantum wire tangentially attached to a superconductor ring threaded by magnetic flux

Ben-Yuan Gu[1,2,a], Yao Lu[1], and Tzong-Jer Yang[2]

[1] Institute of Physics, Academia Sinica, PO Box 603, Beijing 100080, PR China
[2] Department of Electrophysics, National Chiao Tung University, Hsinchu, 30050, Taiwan

Received 6 November 2001

Abstract. We present numerical investigations of the transmission properties of electrons in a normal quantum wire tangentially attached to a superconductor ring threaded by magnetic flux. A point scatterer with a $\delta-$function potential is placed at node to model scattering effect. We find that the transmission characteristics of electrons in this structure strongly depend on the normal or superconducting state of the ring. The transmission probability as a function of the energy of incident electrons, in the case of a superconductor ring threaded by one quantum magnetic flux, emerges one deep dip, imposed upon the first broad bump in spectrum. This intrinsic conductance dip originates from the superconductor state of the ring. When increasing the magnetic flux from one quantum magnetic flux to two, the spectrum shifts toward higher energy region in the whole. This conductance dip accordingly shifts and appears in the second bump. In the presence of a point-scatterer at the node, the spectrum is substantially modified. Based on the condition of the formation of the standing wave functions in the ring and the broken of the time-reserve symmetry of Schrödinger equation after switching magnetic flux, the characteristics of transmission of electrons in this structure can be well understood.

PACS. 73.23.-b Electronic transport in mesoscopic systems – 73.21.Hb Quantum wires – 74.80.Fp Point contact; SN and SNS junctions – 85.35.Ds Quantum interference devices

1 Introduction

In recent years the studies of the transport properties of electrons in normal-conductor-superconductor mesoscopic structures have attracted much attention. The essential feature of mesoscopic physics is the phase coherence of the charge carriers. In the normal mesoscopic structures the transport of electrons retains phase coherence over the phase coherent length L_ϕ. The superconducting state is characterized by a macroscopic wave function, retaining its coherence ideally over arbitrarily large length. The "hybrid" systems with the join of both mesoscopics and supercoductivity bring a plenty of novel physical phenomena [1–5]. Many interesting phenomena have been revealed in various "hybrid" mesoscopic systems, for instance, normal-metal-superconductor (NS) junction, or $S-I-S$, $S-N-S$, $S-I-N$, $N-I-N-S$ junctions [6–11]. Many of the novel characteristics in the NS junction originate from the unusual reflection, known as Andreev reflection [12]: An electron excitation above the Fermi level in the normal metal is reflected at the normal-metal-superconductors (NS) interface as a hole excitation below the Fermi level. The missing charge of $2e$ is converted as a supercurrent [5].

Much of the present technological effort in this area is aimed at fabricating a direct contact between a superconducting film and two-dimensional electron gas (2DEG) in a semiconductor heterostructure. The transport can be made ballistic by employing a high-mobility 2DEG confined in semiconductor heterostructures. Thus, such a "hybrid" system would open the interplay subjects of Andreev reflection and mesoscopic effects [13–15].

The numerical investigations of the electron conductance in a network of wires, such as a quantum waveguide containing an array of stubs, a quantum waveguide topology containing multiply serial-connected mesoscopic rings, or laterally connected dangling mesoscopic rings, have been extensively achieved [16–19]. The conductance as a function of the Fermi wave number of electrons depends on the number of the components and also on physical parameters and geometric configuration of the system. By controlling the related parameters, the conductance spectrum can be artificially tailored.

In this paper we present the quantum mechanical calculations on transmission properties of the "hybrid" quantum network. The model device consists of a main normal

[a] e-mail: guby@aphy.iphy.ac.cn

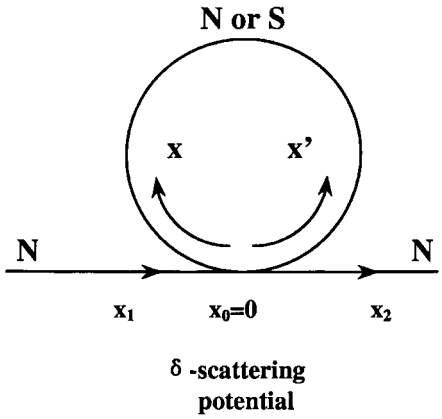

Fig. 1. Schematic diagram of the considered model device. A main conductor quantum wire is tangentially attached to a ring which can be normal conductor or superconductor. A scatterer with the $\delta-$function potential is placed at the junction $x_0 = 0$. The circumference of the ring is L and the magnetic flux is threaded through the ring. The local coordinate system for each branch is indicated. The electrons are injected into the main wire from the left side.

conductor wire tangentially attached to a superconductor ring and a scatterer with the $\delta-$function potential is placed at node to model scattering effect. We find that the transmission properties of electrons in this network strongly depend on the normal or superconducting state of the ring, the geometric size of the ring, the magnetic flux threading through the ring, and the strength of the repulsive or attractive scattering potential. The important finding is that for a superconductor ring pierced one unit quantum magnetic flux, an intrinsic conductance dip emerges in the transmission probability spectrum, imposed upon the first bump. This conductance dip originates from the superconductor state of the ring. Based on physical considerations and discussions, the properties of transportation of electrons in the device can be interpreted well.

This paper is organized as follows: Section 2 presents a brief description of the model device structure and the necessary formulas used in the calculations. The numerical results are presented in Section 3 with analyses. Finally, the discussions and a brief summary are given in Section 4.

2 Model and formulas

The system considered here is a one-dimensional (1D) semiconductor quantum wire tangentially attached to a superconductor ring with a circumference L threading magnetic flux Φ. As a model device, we assume that the wire is narrow enough so that only electron motion in the direction of the wires is of interest. A junction is formed at $x_0 = 0$ and a scatterer with the $\delta-$function potential is placed at this node to model scattering effect. The schematic of the model device is shown in Figure 1. A small voltage is applied to the two ends of the main wire.

First consider the semiconductor wire. In order to match the superconducting ring in the hybrid system, we prefer to employ Nambu space, *i.e.*, the so-called electron-hole space, for describing the motion of quasiparticles in the normal conductor. The phase–coherent transport of the electrons and holes is described by the following equation:

$$\begin{pmatrix} H_0 & 0 \\ 0 & -H_0^* \end{pmatrix} \begin{pmatrix} u_N(x) \\ v_N(x) \end{pmatrix} = E \begin{pmatrix} u_N(x) \\ v_N(x) \end{pmatrix}, \tag{1}$$

where $u_N(x)$ and $v_N(x)$ are the wave functions of the quasiparticles (electrons and holes). The single-particle Hamiltonian is

$$H_0 = \frac{1}{2m_N^*} {p_x}^2 - \mu_N, \tag{2}$$

where μ_N represents the chemical potential of the 2DEG and m_N^* is the effective electron mass in semiconductor, for instance, in GaAs material, $m_N^* = 0.067m_0$, and m_0 denotes the free electron mass. The wave function of quasiparticles in the left main quantum wire separated at the node can be expressed as

$$\Psi_N(x_1) = \begin{pmatrix} 1 \\ 0 \end{pmatrix} \mathrm{e}^{\mathrm{i}k_+ x_1} + A_+ \begin{pmatrix} 1 \\ 0 \end{pmatrix} \mathrm{e}^{-\mathrm{i}k_+ x_1} + B_- \begin{pmatrix} 0 \\ 1 \end{pmatrix} \mathrm{e}^{\mathrm{i}k_- x_1}, \tag{3}$$

where

$$k_\pm = \sqrt{\frac{2m_N^*(\mu_N \pm E)}{\hbar^2}}\,. \tag{4}$$

Here E denotes the energy of incident electrons. In equation (3), the first term describes the incident electrons, the second term corresponds to the electron reflection, and the third term to the hole reflection from the junction. The wave function in the exit of the main quantum wire with the scattering boundary condition can be expressed as

$$\Psi_R(x_2) = D_1 \begin{pmatrix} 1 \\ 0 \end{pmatrix} \mathrm{e}^{\mathrm{i}k_+ x_2} + D_2 \begin{pmatrix} 0 \\ 1 \end{pmatrix} \mathrm{e}^{-\mathrm{i}k_- x_2}. \tag{5}$$

The first term describes the electron transmission and the second term corresponds to the hole transmission.

We now consider the superconductor ring. The phase–coherent transport of the quasiparticle excitations is described by the Bogoliubov-de Gennes equation (BdeG) [20]

$$\begin{pmatrix} H_0 & \Delta(x) \\ \Delta^*(x) & -H_0^* \end{pmatrix} \begin{pmatrix} u(x) \\ v(x) \end{pmatrix} = E \begin{pmatrix} u(x) \\ v(x) \end{pmatrix}, \tag{6}$$

where $u(x)$ and $v(x)$ denote the wave functions of the quasiparticles in superconductor. $\Delta(x)$ is the pair potential. The single-particle Hamiltonian is

$$H_0 = \frac{1}{2m_0}[\mathbf{p} - \frac{e}{c}\mathbf{A}]^2 + V(x) - \mu_S, \tag{7}$$

where $\mathbf{A}$ and $V(x)$ are the vector and scalar potentials, respectively. μ_S is the chemical potential of superconductor. For simplicity, we neglect the self-consistency of the

$$\begin{pmatrix} \left[\frac{1}{2m_0}\left(\frac{\hbar}{\mathrm{i}}\frac{\mathrm{d}}{\mathrm{d}x} \mp \frac{e}{c}\frac{\Phi}{L}\right)^2 + V(x) - \mu_S\right] & \Delta_0 \\ \Delta_0^* & -\left[\frac{1}{2m_0}\left(\frac{\hbar}{-\mathrm{i}}\frac{\mathrm{d}}{\mathrm{d}x} \mp \frac{e}{c}\frac{\Phi}{L}\right)^2 + V(x) - \mu_S\right] \end{pmatrix} \begin{pmatrix} u(x) \\ v(x) \end{pmatrix} = E\begin{pmatrix} u(x) \\ v(x) \end{pmatrix}, \tag{8}$$

$$\det \begin{vmatrix} \left[\frac{\hbar^2}{2m_0}(q \mp \frac{\theta}{L})^2 - \mu_S\right] - E & \Delta_0 \\ \Delta_0^* & -\left[\frac{\hbar^2}{2m_0}(-q \mp \frac{\theta}{L})^2 - \mu_S\right] - E \end{vmatrix} = 0, \tag{10}$$

pair potential Δ, and assume that $\Delta(x) = \Delta_0 = \text{const.}$ in superconductor. When the wire width is small compared to the superconducting coherence length $\xi = \hbar v_F/(2\Delta_0)$ (which represents the size of the Cooper pair), or when the resistivity of the semiconductor is larger than the normal resistivity of the superconductor, this approximation is appropriate. The magnetic flux is assumed to be threaded into the superconducting ring. Thus, we have $\mathbf{A} = (0, A_\theta, 0)$ and $A_\theta = \Phi/2\pi R = \Phi/L$, R is the radius of the ring. Φ represents the magnetic flux threading through the ring, $\Phi = BS$, B is the magnitude of magnetic field perpendicular to the ring plane, S is the surrounded area by the ring.

In order for the convenience of calculations, we introduce the local coordinate system for each circuit such that the direction is along the electron-current direction and the origin is taken at the intersection of the left branch of the ring with the main wire, as shown in Figure 1, the arrows indicate the assuming direction of electron-current at each branch. In the local coordinate system, the BdeG equation reads as follows:

See equation (8) above

where sign $\mp$ corresponds to the left-half/right-half ring. We assume that the solution takes a form of

$$\begin{pmatrix} u(x) \\ v(x) \end{pmatrix} = \begin{pmatrix} \alpha \\ \beta \end{pmatrix} \mathrm{e}^{\mathrm{i}qx}, \tag{9}$$

and we substitute this formal solution into equation (8), then we derive an equation for determining the wave number q

See equation (10) above

where we set $V(x) = 0$ for simplicity and $\theta = 2\pi\Phi/\phi_0$; $\phi_0 = hc/e$ is the quantum magnetic flux. Thus, we obtain an algebraic equation for determining q as

$$\widetilde{q}^4 - 2\widetilde{q}^2\left[(\frac{\theta}{q_F L})^2 + 1\right] \mp 2\widetilde{q}\frac{\theta}{q_F L}\widetilde{E} + \left[(\frac{\theta}{q_F L})^2 - 1 - \widetilde{E}^2 + |\widetilde{\Delta}_0|^2\right] = 0. \tag{11}$$

Here, we introduce $\widetilde{q} = q/q_F$, $\widetilde{E} = E/\mu_S$, $\widetilde{\Delta}_0 = \Delta_0/\mu_S$, and $q_F = \sqrt{2m_0\mu_S}/\hbar$.

Solving equation (11), we can obtain four roots $q_\pm^{(\pm)}$. They correspond to the positive ($q_+^{(+)}$) or negative ($q_+^{(-)}$) group velocity of electronlike excitations, similarly, the positive ($q_-^{(+)}$) or negative ($q_-^{(-)}$) group velocity of holelike excitations. The corresponding wave functions are

$$\begin{pmatrix} u(x) \\ v(x) \end{pmatrix} = \begin{pmatrix} \alpha_\pm^{(\pm)} \\ \beta_\pm^{(\pm)} \end{pmatrix} \mathrm{e}^{\mathrm{i}q_\pm^{(\pm)}x}. \tag{12}$$

The wave functions are required to be normalized.

In order to avoid solving this fourth order algebraic equation, we prefer to use another approach to determine q. For the left-half superconducting ring, equation (8) can be written explicitly as

$$\left[(\widetilde{q} - \frac{\theta}{q_F L})^2 - 1 - \widetilde{E}\right] u^{(\text{left})}(x) + \widetilde{\Delta}_0 v^{(\text{left})}(x) = 0, \tag{13a}$$

and

$$\left[(\widetilde{q} + \frac{\theta}{q_F L})^2 - 1 + \widetilde{E}\right] v^{(\text{left})}(x) - \widetilde{\Delta}_0^* u^{(\text{left})}(x) = 0. \tag{13b}$$

Equations (13a) and (13b) can be simply solved by use of an expanded basis approach [21,22] (u, v, $\widetilde{u} = \widetilde{q}u$, $\widetilde{v} = \widetilde{q}v$). We can easily derive an eigen equation as

$$\begin{pmatrix} 0 & 0 & 1 & 0 \\ 0 & 0 & 0 & 1 \\ \left[-(\frac{\theta}{q_F L})^2 + 1 + \widetilde{E}\right] & -\widetilde{\Delta}_0 & \frac{2\theta}{q_F L} & 0 \\ \widetilde{\Delta}_0^* & \left[-(\frac{\theta}{q_F L})^2 + 1 - \widetilde{E}\right] & 0 & -\frac{2\theta}{q_F L} \end{pmatrix} \times \begin{pmatrix} u \\ v \\ \widetilde{u} \\ \widetilde{v} \end{pmatrix} = \widetilde{q}\begin{pmatrix} u \\ v \\ \widetilde{u} \\ \widetilde{v} \end{pmatrix}. \tag{14}$$

For a given incident energy $\widetilde{E}$, we can obtain a set of eigen wave numbers $\{\widetilde{q}_\pm^{(\pm)}\}$ and the corresponding eigen

$$\begin{pmatrix} \binom{-1}{0} & \binom{0}{-1} & \binom{0}{0} & \binom{0}{0} & \binom{0}{0} & \binom{0}{0} & \binom{1}{0} & \binom{0}{1} \\ \binom{-1}{0} & \binom{0}{-1} & \binom{\alpha_+^{(+)}}{\beta_+^{(+)}} & \binom{\alpha_+^{(-)}}{\beta_+^{(-)}} & \binom{\alpha_-^{(+)}}{\beta_-^{(+)}} & \binom{\alpha_-^{(-)}}{\beta_-^{(-)}} & \binom{0}{0} & \binom{0}{0} \\ \binom{-1}{0} & \binom{0}{-1} & b_+^{(+)} & b_+^{(-)} & b_-^{(+)} & b_-^{(-)} & \binom{0}{0} & \binom{0}{0} \\ c_1 & c_2 & a_+^{(+)} & a_+^{(-)} & a_-^{(+)} & a_-^{(-)} & \frac{m_0}{m_N^*}\widetilde{k}_+\binom{1}{0} & (-\frac{m_0}{m_N^*}\widetilde{k}_-)\binom{0}{1} \end{pmatrix} \begin{pmatrix} A_+ \\ B_- \\ C_+^{(+)} \\ C_+^{(-)} \\ C_-^{(+)} \\ C_-^{(-)} \\ D_1 \\ D_2 \end{pmatrix} = \begin{pmatrix} \binom{1}{0} \\ \binom{1}{0} \\ \binom{1}{0} \\ (\frac{m_0\widetilde{k}_+}{m_N^*} - \mathrm{i}q_F L\widetilde{Z})\binom{1}{0} \end{pmatrix}, \tag{20}$$

wave functions

$$\begin{pmatrix} u_\pm^{(\pm)}(x) \\ v_\pm^{(\pm)}(x) \end{pmatrix} = \begin{pmatrix} \alpha_\pm^{(\pm)} \\ \beta_\pm^{(\pm)} \end{pmatrix} \mathrm{e}^{\mathrm{i}\widetilde{q}_\pm^{(\pm)} q_F x}. \tag{15}$$

In the local coordinate system, the wave function of quasiparticles at the left-half superconductor ring can be expressed as

$$\begin{aligned} \Psi_S^{(\mathrm{left})}(x) = {} & C_+^{(+)} \begin{pmatrix} \alpha_+^{(+)} \\ \beta_+^{(+)} \end{pmatrix} \mathrm{e}^{\mathrm{i}\widetilde{q}_+^{(+)}\widetilde{x}} + C_+^{(-)} \begin{pmatrix} \alpha_+^{(-)} \\ \beta_+^{(-)} \end{pmatrix} \mathrm{e}^{\mathrm{i}\widetilde{q}_+^{(-)}\widetilde{x}} \\ & + C_-^{(+)} \begin{pmatrix} \alpha_-^{(+)} \\ \beta_-^{(+)} \end{pmatrix} \mathrm{e}^{\mathrm{i}\widetilde{q}_-^{(+)}\widetilde{x}} + C_-^{(-)} \begin{pmatrix} \alpha_-^{(-)} \\ \beta_-^{(-)} \end{pmatrix} \mathrm{e}^{\mathrm{i}\widetilde{q}_-^{(-)}\widetilde{x}}; \end{aligned} \tag{16a}$$

and for the right-half ring, it is

$$\begin{aligned} \Psi_S^{(\mathrm{right})}(x') = {} & C_+^{(+)} \begin{pmatrix} \alpha_+^{(+)} \\ \beta_+^{(+)} \end{pmatrix} \mathrm{e}^{\mathrm{i}\widetilde{q}_+^{(+)}\widetilde{L}} \mathrm{e}^{-\mathrm{i}\widetilde{q}_+^{(+)}\widetilde{x}'} \\ & + C_+^{(-)} \begin{pmatrix} \alpha_+^{(-)} \\ \beta_+^{(-)} \end{pmatrix} \mathrm{e}^{\mathrm{i}\widetilde{q}_+^{(-)}\widetilde{L}} \mathrm{e}^{-\mathrm{i}\widetilde{q}_+^{(-)}\widetilde{x}'} \\ & + C_-^{(+)} \begin{pmatrix} \alpha_-^{(+)} \\ \beta_-^{(+)} \end{pmatrix} \mathrm{e}^{\mathrm{i}\widetilde{q}_-^{(+)}\widetilde{L}} \mathrm{e}^{-\mathrm{i}\widetilde{q}_-^{(+)}\widetilde{x}'} \\ & + C_-^{(-)} \begin{pmatrix} \alpha_-^{(-)} \\ \beta_-^{(-)} \end{pmatrix} \mathrm{e}^{\mathrm{i}\widetilde{q}_-^{(-)}\widetilde{L}} \mathrm{e}^{-\mathrm{i}\widetilde{q}_-^{(-)}\widetilde{x}'}, \end{aligned} \tag{16b}$$

where $\widetilde{q}_\pm^{(\pm)} = q_\pm^{\pm)}/q_F$, $\widetilde{x} = q_F x$, $\widetilde{x}' = q_F x'$, and $\widetilde{L} = q_F L$. The amplitude of coefficients, A_+, B_-, $C_\pm^{(\pm)}$, D_1, and D_2, are determined by the continuity of the wave function and the general Kirchhoff's current law (KCL) [23,24]. The general KCL requires that at each node the sum of the quantities $\frac{1}{m^*}\psi^*(\mathrm{i}\nabla + 2\pi\mathbf{A}/\phi_0)\psi$ from all the individual branches must be zero. It follows

$$\sum_j \frac{1}{m_j^*}\left[\mathrm{i}\frac{\partial}{\partial l} + \frac{2\pi A_j(l)}{\phi_0}\right]\psi_j(l)\Big|_{l=x_0} = \frac{2}{\hbar^2} Z\psi(x_0). \tag{17}$$

Here we model the scattering at the junction by a $\delta-$function potential

$$U(x) = Z\delta(x), \tag{18}$$

where Z is the strength of the scattering potential. Thus, we have

$$\Psi_N(0) = \Psi_S^{(\mathrm{left})}(0) = \Psi_R(0), \;\; \Psi_S^{(\mathrm{right})}(0) = \Psi_S^{(\mathrm{left})}(L); \tag{19a}$$

$$\frac{1}{m_N^*}\frac{\mathrm{d}\Psi_R}{\mathrm{d}x} + \frac{1}{m_0}\left[\frac{\mathrm{d}\Psi_S^{(\mathrm{left})}}{\mathrm{d}x} + \frac{\mathrm{d}\Psi_S^{(\mathrm{right})}}{\mathrm{d}x}\right] - \frac{1}{m_N^*}\frac{\mathrm{d}\Psi_N}{\mathrm{d}x} = \frac{2}{\hbar^2} Z\Psi_N, \;\; at \;\; x_0 = 0, \tag{19b}$$

because $A^{(\mathrm{left})}(x_0) = -A^{(\mathrm{right})}(x_0) = \Phi/L$; they are cancelled each other.

Finally, we can derive the following equation for determining the related coefficients in a matrix form:

See equation (20) above

where

$$a_\pm^{(\pm)} = \widetilde{q}_\pm^{(\pm)}(1 - \mathrm{e}^{\mathrm{i}\widetilde{q}_\pm^{(\pm)}\widetilde{L}}) \begin{pmatrix} \alpha_\pm^{(\pm)} \\ \beta_\pm^{(\pm)} \end{pmatrix}; \tag{21a}$$

$$b_\pm^{(\pm)} = \mathrm{e}^{\mathrm{i}\widetilde{q}_\pm^{(\pm)}\widetilde{L}} \begin{pmatrix} \alpha_\pm^{(\pm)} \\ \beta_\pm^{(\pm)} \end{pmatrix}; \tag{21b}$$

$$c_1 = (\frac{m_0\widetilde{k}_+}{m_N^*} + \mathrm{i}q_F L\widetilde{Z}) \begin{pmatrix} 1 \\ 0 \end{pmatrix}; \tag{21c}$$

$$c_2 = (-\frac{m_0\widetilde{k}_-}{m_N^*} + \mathrm{i}q_F L\widetilde{Z}) \begin{pmatrix} 0 \\ 1 \end{pmatrix}; \tag{21d}$$

$$c_3 = (\frac{m_0\widetilde{k}_+}{m_N^*} - \mathrm{i}q_F L\widetilde{Z}) \begin{pmatrix} 1 \\ 0 \end{pmatrix}. \tag{21e}$$

Here we introduced the dimensionless quantities: $\widetilde{k}_\pm = k_\pm/q_F$, $\widetilde{Z} = Z/(\mu_S L)$.

The reflection and transmission probabilities for the incident electrons are related to the above mention coefficients as

$$R_{ee} = (|v_+^{(-)}|/v_+^{(+)})|A_+|^2; \tag{22a}$$

$$R_{he} = (|v_-^{(-)}|/v_+^{(+)})|B_-|^2; \tag{22b}$$

$$T_{ee} = (|v_+^{(+)}|/v_+^{(+)})|D_1|^2; \tag{22c}$$

$$T_{he} = (|v_-^{(+)}|/v_+^{(+)})|D_2|^2. \tag{22d}$$

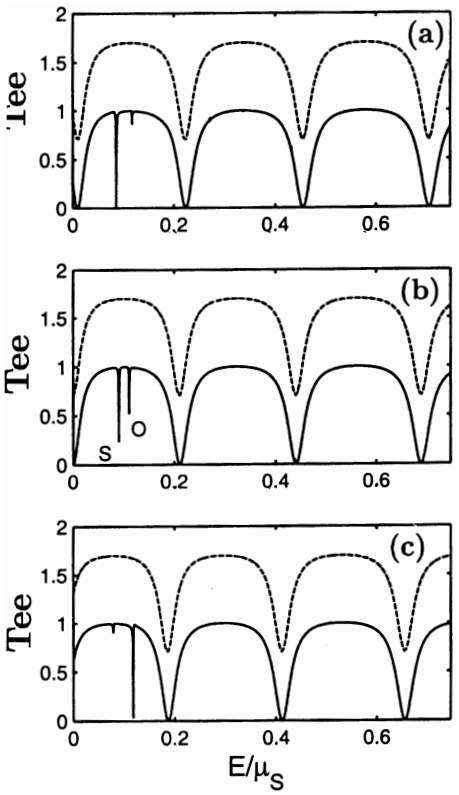

Fig. 2. Typical spectra of transmission probabilities of electrons as a function of the energy of incident electrons for different $q_F L$. The quantum magnetic flux threading through the ring is $\theta/\pi = 1.0$. The parameters used are: $m_N^* = 0.067m_0$, $\mu_N = \mu_S$, $\widetilde{Z} = 0.0$; (a) for $q_F L = 19.9\pi$, (b) for $q_F L = 20.0\pi$, and (c) for $q_F L = 20.2\pi$. All solid curves correspond to superconductor ring with $\widetilde{\Delta}_0 = 0.02$ and dashed curves to normal metal ring. Two curves in each plot have been separated vertically by 0.7 for clarity. The marked 'S' indicates the intrinsic conductance dip related to the superconductor state and 'O' indicates the dip belonging to the occasional lift of the degenerate eigen energy of electrons in the ring.

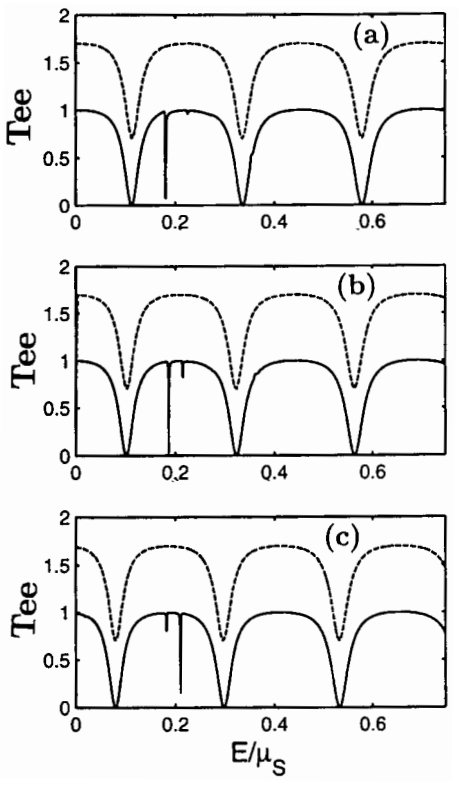

Fig. 3. Same as Figure 2 except for $\theta/\pi = 2.0$. (a) for $q_F L = 19.9\pi$, (b) for $q_F L = 20.0\pi$, and (c) for $q_F L = 20.2\pi$. All solid curves correspond to the superconductor ring.

Here $v_{\pm}^{(\pm)}$ is the velocity of quasiparticles. For this particular system, we have

$$R_{he} = T_{he}.$$

Note that the probability conservation requires

$$\left[R_{ee} + R_{eh} + T_{ee} + T_{he}\right] = 1. \tag{23}$$

3 Results and analyses

To reveal the character of this model device, we now calculate the transmission probability T_{ee} as a function of energy (E/μ_S) of the incident electrons for several values of $q_F L$ and different magnetic flux. The results are displayed in Figures 2 and 3. The parameters used in calculations are: $m_N^* = 0.067m_0$, $\mu_N = \mu_S$, without the scattering, *i.e.*, $\widetilde{Z} = 0$: (a) for $q_F L = 19.9\pi$ and $\theta/\pi = 1.0$; (b) for $q_F L = 20.0\pi$ and $\theta/\pi = 1.0$; and (c) for $q_F L = 20.2\pi$ and $\theta/\pi = 1.0$. Figures 3(a–c) just are the analogous to Figures 2(a–c) except for $\theta/\pi = 2.0$. For a superconductor loop, the magnetic flux Φ threading through its hole should be taken a series of discrete quantization values: $\Phi/\phi_{s0} = n$, $\phi_{s0} = hc/2e = \phi_0/2$ is the quantum flux for Cooper pair; thus $\theta = 2\pi\Phi/\phi_0 = n\pi$, $n = 1, 2, 3...$ All dashed curves correspond to the case of the normal metal ring (*i.e.*, $\widetilde{\Delta}_0 = 0$), while all solid curves correspond to the superconducting state of ring with $\widetilde{\Delta}_0 = \Delta_0/\mu_S = 0.02$. Two curves in each plot have been separated by 0.7 for clarity. The marked 'S' in Figure 2b indicates the conductance dip related to the supercoductor state and 'O' indicates the conductance dip belonging to the occasional lift of the original degenerate eigen energy of electrons in the ring. It is clearly seen from these plots that for the normal metal ring pierced through an exact quantization quantum flux of $\theta/\pi = 1$, or 2, the transmission probability spectrum exhibits periodically oscillatory behavior. When changing θ/π from 1.0 to 2.0, the spectrum only produces a simple shift to right in the whole. When the ring becomes the superconductor state and a unit quantum magnetic flux is pierced its hole, a novel phenomenon takes place: A narrow and deep conductance dip emerges, imposed upon the first broad bump, as shown in Figures 2a, b, and c (solid lines). It is worth emphasizing that this conductance dip is not observed in the next or any further bumps.

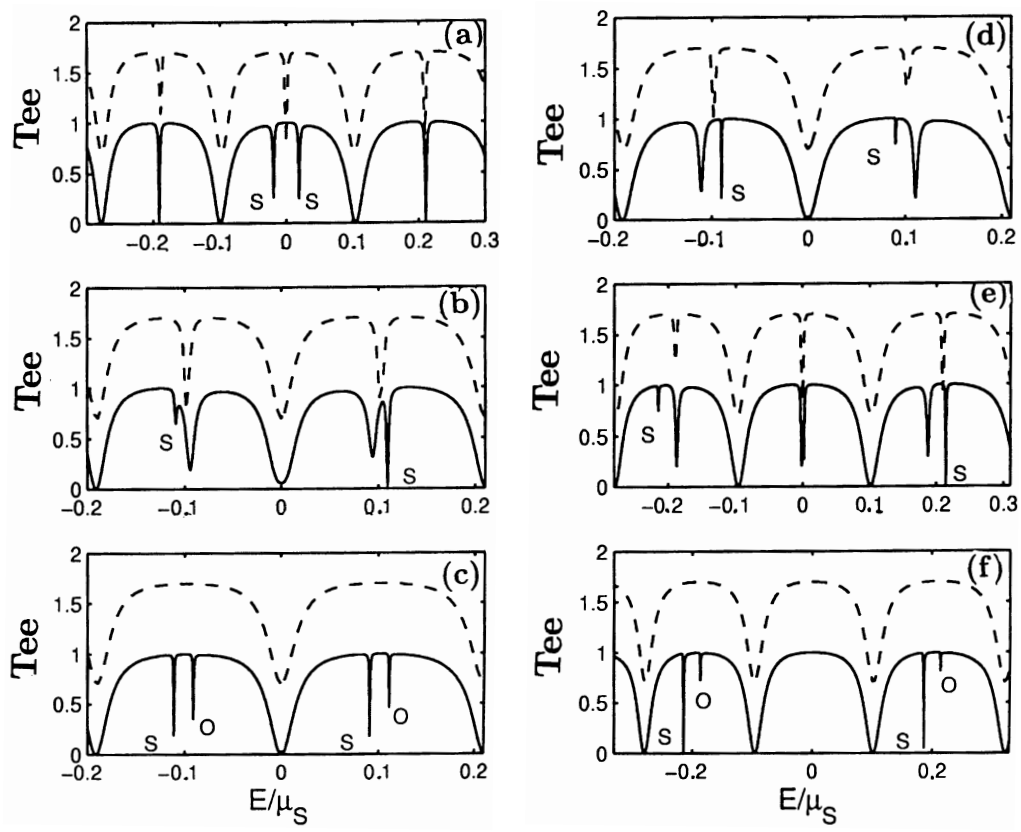

Fig. 4. Evolution of spectra of transmission probabilities of electrons as a function of the energy of incident electrons with the gradual increase of magnetic flux. The relevant parameters used are as follows: $q_F L = 20.0\pi$; $\widetilde{\Delta}_0 = 0.02$; $\mu_N = \mu_S$; $m_N^* = 0.067m_0$; $\widetilde{Z} = 0.0$; (a) $\theta/\pi = 0.17$; (b) $\theta/\pi = 0.73$; (c) $\theta/\pi = 1.0$; (d) $\theta/\pi = 1.17$; (e) $\theta/\pi = 1.85$; and (f)$\theta/\pi = 2.0$. All solid curves correspond to the superconductor ring with $\widetilde{\Delta}_0 = 0.02$ and dashed curves to the normal metal ring. Two curves in each plot have been separately by 0.7 for clarity. The marked 'S' indicates the conductance dip related to the superconductor state and 'O' indicates the dip belonging to the occasional lift of the degenerate eigen energy of electrons in the ring .

This is fully different from the conventional conductance dip produced by the magnetic splitting of the degenerate eigen states in the ring; the conventional conductance dips always emerge in every broad bump of the transmission probability spectrum. Therefore, hereafter we refer this special conductance dip to the intrinsic conductance dip strongly related to the superconductor state of ring. The position of conductance dip strongly depends on the geometrical size of the ring, circumference of L. When decreasing (or increasing) $q_F L$ from $q_F L = 20.0\pi$, the conductance dip shifts toward lower (see Fig. 2a) (or higher, see Fig. 2c) energy region. In addition, in comparison to normal metal ring, with the exception of this intrinsic conductance dip, there is another shallower conductance dip occurred inside the first bump, which is marked by 'O' in Figure 2b for the recognition. We also employ these marks in other figures. The occurrence of this conductance dip is occasional, we will discuss it in the next paragraph for details. This occasional conductance dip differs completely from the conventionally magnetic producing dip appearing in every bump. When introducing a small perturbation in $q_F L$ or θ, this dip can disappear. When increasing θ/π from 1.0 to 2.0, the profile of the spectrum is varied as follows: The zero transmission at zero energy point in spectrum converts into a unity transmission peak (see, Figs. 2b and 3b), accordingly, the spectrum looks like to do a simple shift to right in the whole. Consequently, the dip now appears in the second bump owing to this whole shift.

To sufficiently reveal the physical origin of this intrinsic transmission dip, we first artificially switch much weak magnetic flux threading through the ring and then gradually increase the flux step by step. We carefully envisage the evolution of the transmission probability spectra of electrons. The results are displayed in Figure 4. In order to present a full insight, we plot all the figures from the negative energy (for the holelike quasiparticles) to the positive energy (for the electronlike quasiparticles). The relevant parameters used in calculations are as follows: $q_F L = 20.0\pi$; $\mu_N = \mu_S$; $m_N^* = 0.067m_0$; $\widetilde{Z} = 0.0$; (a) $\theta/\pi = 0.17$; (b) $\theta/\pi = 0.73$; (c) $\theta/\pi = 1.0$; (d) $\theta/\pi = 1.17$; (e) $\theta/\pi = 1.85$; and (f)$\theta/\pi = 2.0$. All solid curves correspond to the superconductor ring with $\widetilde{\Delta}_0 = 0.02$ and dashed curves to the normal metal ring. Two curves in each plot have been separated by 0.7 for clarity. At zero flux, the conductance spectra for both normal and superconductor rings exhibit almost the same behavior, they

display conventionally periodical oscillations. As well discussed in references [16–19], T_{ee} unity peaks in spectra are completely determined by the eigenstates of electrons survived in the ring. At zero flux or integer multiple of quantum magnetic flux, the eigenstate of the electrons with clockwise and counterclockwise travels is two–fold degenerate, consequently, the conductance spectrum almost retains similar. When we increase the flux by one (two) quantum magnetic flux, the conductance spectrum simply shifts toward higher energy region by one (two) period 0.1 (0.2) for electronlike quasiparticles ($E > 0$) (or lower energy region for holelike quasiparticles ($E < 0$)) in the whole, as seen in Figures 4c and f. However, when the flux threading through the loop is non-integer multiple of the quantum magnetic flux, a narrow and deep conductance dip occurs inside every broad bump. Thus, each originally complete bump now splits into two components separated by a deep conductance dip, as shown in Figures 4a, b, d, and e (dashed lines). As the magnetic-field breaks the time-reversal symmetry of the Schrödinger equation, therefore, the degeneracy of the original two-fold degenerate-eigenstates of electrons, corresponding to the clockwise and counterclockwise travels of electrons in the ring, now is lifted. It leads to the splitting of the spectrum. Therefore, when switching small magnetic flux, for instance, $\theta/\pi = 0.17$, this trivial magnetic splitting in spectrum takes place in both cases of normal and superconductor rings. Every bump splits into two components. However, it is noted that the central part of spectrum around the zero energy point now occurs a substantial change (see Fig. 4a). For the normal ring, there exists a conventional conductance dip belonging to the magnetic splitting of the degenerate eigen states, as shown by the dashed line in Figure 4a, on the contrary, in the case of superconductor ring, this conductance dip completely disappears, replaced by a unity peak. Meanwhile, two narrow and deep conductance dips, marked by 'S', are brought about and symmetrically located at two sides of the zero energy point, as shown by the solid line in Figure 4a. We may have some evidences to believe that these two conductance dips definitely originate from the superconductor state. Their energy positions E_S/μ_S are ± 0.01914, very close to $\widetilde{\Delta}_0 = 0.02$. As increasing $\widetilde{\Delta}_0$, the absolute values of their energy positions are increased. For instance, $|E_s/\mu_S| = 0.03818, 0.04776, 0.05737$ correspond to $\widetilde{\Delta}_0 = 0.04, 0.05, 0.06$, respectively, very close to their relevant pair potential. The second evidence is that this intrinsic conductance dip only occurs in the first bump, numbering from zero energy point. It fully differs from the conductance dip related to the usually magnetic splitting of spectrum, appearing in every bump. In contrast, this intrinsic conductance dip only lies in the central bump now. The third evidence is that when the energy of the incident electrons can be comparable with $\widetilde{\Delta}_0$, the coupling effect owing to the presence of pair potential may lead to a phase compensation of the wave function, thus, the normal conductance dip produced the magnetic splitting now is converted into a unity peak. When increasing the flux, from $\theta/\pi = 0.17$ to 0.73, the spectrum over the positive energy range shifts to right in the whole. There exist two conductance dips in the first bump of the spectrum now, one broad dip corresponds to the magnetic splitting of the spectrum, in comparison with the spectrum of the normal ring. The other conductance dip with much narrow width, marked by 'S', should be ascribed to the superconductor state. This intrinsic conductance dip is developed from 'S' dip of Figure 4a. The original central bump containing the 'S' dip now shifts in the whole toward higher energy region and becomes the first bump in Figure 4b. As continuously enhancing θ/π, arriving at 1.0, one unit quantum magnetic flux (see, Fig. 4c), the eigen states are recovered two fold degeneracy. Thus, the magnetic spitting of spectrum disappears for the normal ring and the corresponding spectrum looks like to make a shift in the whole toward higher energy region by one period 0.1 for the electronlike quasiparticles, as shown by the dashed line in Figure 4c. However, for the superconductor ring, two deep conductance dips, marked by 'S' and 'O', occur in the first bump (see Fig. 4c, solid line). The occurrence of 'O' conductance dip is produced by the influence of the pair potential, leading to the occasional splitting of spectrum. The survival of this dip is relatively unstable and much sensitive to the weak fluctuation of the parameters of structure. For instance, by introducing a small perturbation of $q_F L$ or θ , this dip becomes much shallow or can be eliminated completely. The other deep dip, marked by 'S', is related to the nature of the superconductor states, which is relatively robust and stable to the perturbation of the parameters of system, only sensitive to the phase transition between the normal and superconductor states. Consequently, we easily judge and distinguish them: Which one is 'O' or 'S' dip. When we further continuously increase the flux toward $\theta/\pi = 2.0$, the spectrum shifts to higher energy region in the whole, and the intrinsic dip always is survived in the first bump, as shown in Figures 4d–f. Finally, at $\theta/\pi = 2.0$, the conductance dip associated with the magnetic splitting of spectrum disappears again. The intrinsic dip now lies on the second bump, numbering from the zero energy point, owing to the whole shift of the spectrum.

These results can be well interpreted based on the following physical discussions. For the normal metal ring, when an electron with the energy E is injected into a ring of the circumference L, at zero flux, the condition of the occurrence of the standing wave is $\mathrm{e}^{\mathrm{i}q_n L} = \mathrm{e}^{\mathrm{i}2n\pi} = 1$, where n is an integer number and $q_n/q_F = \sqrt{1 + E_n/\mu_S}$. When we choose $L = 20.0\pi/q_F$ and the wave number of the injected electron just is $q = q_F$, (*i.e.*, $E = 0$), therefore, we have $qL = q_F L = 20.0\pi$, a standing wave is formed now; electrons always are favorable to reside in this eigen state of the ring. Since at zero flux, the eigen state of $\pm q_n$ associated with E_n is two-fold degenerate; for each E_n there are two currents flowing through the ring: one is clockwise and other is counterclockwise. Both they have the same magnitude, therefore, the net current flowing through the ring vanishes. Apparently, the incident electrons do not feel the existence of the ring at zero flux. Therefore, T_{ee} should be equal unity. However, as soon as switching any small flux, the magnetic field breaks the

time-reverse symmetry of the Schrödinger equation, thus, the originally two-fold degenerate eigen states now are lifted. It leads to the clockwise and counterclockwise currents in the ring can not be cancelled with each other and it results in a net current flowing through the ring. Consequently, T_{ee} becomes zero, a unity-depth dip emerges at zero energy point for any weak flux, as seen in the dashed line in Figure 4a.

We now turn to discuss the situation of the superconducting ring. The difference between two cases lies in the fact that the superconductor possesses a finite pair potential of Δ_0. Thus, the quasiparticles – electronlike and holelike – are coupled each other by this pair potential. The dispersion relation of electronlike quasiparticles in superconductor at zero magnetic flux is given by

$$q/q_F = \sqrt{1 + \sqrt{(E^2 - |\Delta_0|^2)}/\mu_S}.$$

Consequently, for a given q, there exist two values of energy $\pm E_S$. Only when q is real, the state corresponds to non-decaying state. The condition of the creation of the eigen states still requires $qL = 2n\pi$. For a given $L = 20.0\pi/q_F$ and $qL = 20.0\pi$, there exist two eigen states with the energies $\pm E_S$, which satisfy $\sqrt{1 + \sqrt{(E_s^2 - |\Delta_0|^2)}/\mu_S} = q/q_F = 1$. At zero flux, for each $|E_S|$, there exist clockwise and counterclockwise currents corresponding to $\pm q$. They are cancelled with each other, leading to zero net current in the ring, thus, T_{ee} takes unity. However, when switching small magnetic flux, owing to the broken of the time-reverse symmetry of the Schrödinger equation, the originally two-fold degenerate states associated with $\pm q$ are lifted. It causes a net persistent current flowing in the ring. Thus, two dips in spectrum should emerge at the symmetric energy positions with respect to zero energy point, $\pm E_S$, as shown by solid curve in Figure 4a. When $q_F L$ deviates from 20.0π, for instance, $q_F L = 19.9\pi$ (or 20.2π), in order to match the condition of the formation of the standing waves in the ring, $qL = 2n\pi$, it needs to compensate (or extract) a deficit (or extra quantity) of the phase and requires $q/q_F = 20.0/19.9 > 1$ (or $q/q_F = 20.0/20.2 < 1$). Thus, the first zero point of T_{ee} should appear at $q > q_F$ (or $q < q_F$) energy position, as shown in Figure 2a (or Fig. 2c). Therefore, the first conductance bump shifts to right or left, accordingly. This intrinsic conductance dip then shifts to left (see, Fig. 2a) (or right, see Fig. 2c), comparing to the case of $q_F L = 20.0\pi$ (see, Fig. 2b) visually.

We now study the effect of the scatterer placed at the node on the transmission spectrum. The scattering effect is modelled by a $\delta-$function potential with the strength of Z. Spectra of transmission probabilities of electrons for different strengths of repulsive ($\widetilde{Z} > 0$) (attractive $\widetilde{Z} < 0$) scattering potentials are displayed in Figure 5. The parameters are: $\mu_N = \mu_S$; $q_F L = 20.2\pi$; $m_N^* = 0.067 m_0$; $\theta/\pi = 1.0$. (a) for $\widetilde{Z} = +0.05$; (b) for $\widetilde{Z} = +0.08$; and (c) for $\widetilde{Z} = +0.10$. All solid curves correspond to the superconductor ring with $\widetilde{\Delta}_0 = 0.02$ and dashed curves to the normal ring. Two curves in each plot have been separately by 0.7 for clarity. The magnified plots of transmission probability spectra around the intrinsic dip are shown in Figure 6: (a2) for $\widetilde{Z} = \pm 0.05$; (b) for $\widetilde{Z} = \pm 0.08$; and (c) for $\widetilde{Z} = \pm 0.10$. Two curves have been separated vertically for clarity. It is clearly seen from these curves that the spectra exhibit saw-tooth oscillations with the same period as that without scatterer. The intrinsic conductance dip can be observed in all plots. The energy position of the conductance dip is not affected with the change of the scattering strength and the type of scattering potential: repulsive or attractive potential, as shown in Figures 6 (a–c). The effect of the scattering on the spectrum only leads to a decrease of T_{ee} magnitude with the increase $|\widetilde{Z}|$. Meanwhile, when we replace the repulsive scattering potential by an attractive potential, it is found that the inclined direction of each bump in the spectra is reversed.

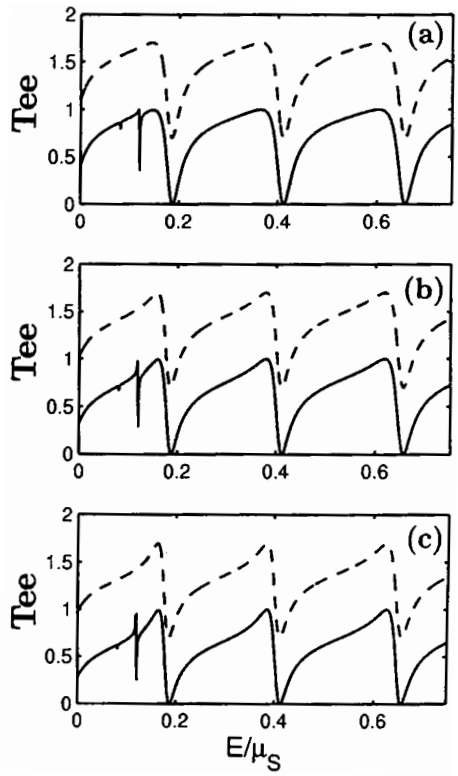

Fig. 5. Spectra of transmission probabilities of electrons for different strengths of repulsive ($\widetilde{Z} > 0$) scattering potential. The parameters are: $\mu_N = \mu_S$; $q_F L = 20.0\pi$; $m_N^* = 0.067 m_0$; $\theta/\pi = 1.0E$. (a) for $\widetilde{Z} = +0.05$; (b) for $\widetilde{Z} = +0.08$; and (c) for $\widetilde{Z} = +0.10$. All solid curves correspond to the superconductor ring with $\widetilde{\Delta}_0 = 0.02$ and dashed curves to the normal ring. Two curves in every plot have been separated by 0.7 for clarity.

4 Discussions and summary

For simplicity, we employ a $\delta-$function potential with a single parameter Z to model the scattering effect at the junction phenomenologically. If the junction possesses some spatial structures, this $\delta-$function scattering potential still keeps effective. Referring to our previous paper,

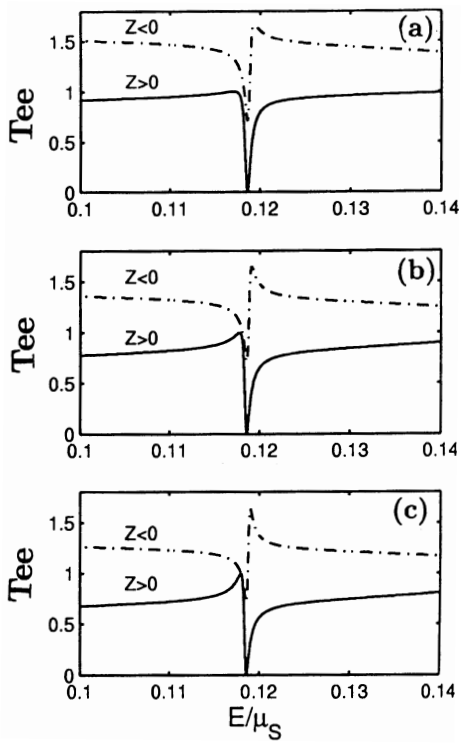

Fig. 6. Magnified plot of transmission probability spectra around the intrinsic dip for different strengths of repulsive ($\widetilde{Z} > 0$) (attractive $\widetilde{Z} < 0$) scattering potential; (a) for $\widetilde{Z} = \pm 0.05$; (b) for $\widetilde{Z} = \pm 0.08$; and (c) for $\widetilde{Z} = \pm 0.10$. Two curves have been separated for clarity.

[25] we can introduce impedance factors for geometric and potential scatterers and develop a recursive algorithm. We find that the impedance factor Z of a complicated side-branch structure can be evaluated from impedance factors of the individual parts contained in the structure as in the classical resistance-network calculation. Finally, the complex junction structures can be stimulated by a $\delta-$function potential after introducing the corresponding impedance factor as the potential strength.

In summary, we have presented numerical investigations of the transmission properties of electrons in the model device which consists of a main quantum wire tangentially attached to a ring. The ring can be normal metal or superconductor, and the magnetic flux threads through this ring, as well as a scatterer is placed at the node. We display the transmission probability spectra as a function of the energy of the incident electron for various geometric and physical parameters. We find that the spectra strongly depend on the normal or superconductor state of ring. When introducing unit quantum magnetic flux, for the normal ring, the transmission probability spectra display usually periodical oscillations. However, for the superconductor ring, an intrinsic conductance dip occurs, imposed upon the first bump of the spectrum. This conductance dip always is survived in the spectra, regardless of the change of magnetic flux, the geometric size of the ring, and the scattering effect. The energy position of this dip depends on the circumference of ring and magnetic flux. When increasing the magnetic flux, from $\theta/\pi = 1.0$ to 2.0, the spectrum almost remains similar pattern except for a simple shift toward higher energy region in the whole. This intrinsic conductance dip is relatively robust and stable to the perturbation of physical and geometric parameters of system, only sensitive to the phase transition between the normal and superconductor states. In the presence of the scatterer with the $\delta-$function potential at the node, the spectra become periodically modulated function with the inclined bump unit, and the intrinsic conductance dip still is survived. The energy position of the conductance dip is not affected with the change of the scattering strength, regardless of repulsive or attractive potential. When changing the the type of scattering potential, from repulsive to attractive, the inclined direction of each unit bump in the spectra is reversed. Based on the condition of the formation of the standing waves in the ring and the consideration of the broken of the time-reverse symmetry of the Schrödinger equation after introducing any small magnetic flux, these main findings can be interpreted well. We also reveal the nature of this intrinsic conductance dip and its origin, from the studies of the detailed evolution of spectra with the gradual increase of magnetic flux. We provide some appropriate supports to confirm the fact that the intrinsic conductance dip indeed originates from the superconductor state.

One of authors (B.Y. Gu) is grateful for the hospitality of the National Science Council, Taiwan and the Electrophysics Department, National Chiao Tung University, Hsinchu, Taiwan. This work was supported by the National Science Council of the Republic of China through Grant No. NSC 88-2112-M-009-003 and the National Natural Science Foundation of China.

References

1. H. Kroemer, M. Thomas, Superlattices Microstruct. **21**, 61 (1997).
2. A.F. Volkov, A.V. Zaitsev, Phys. Rev. B **53**, 9267 (1996).
3. N.R. Claughton, M. Leadbeater, C.J. Lambert, J. Phys. Cond. Matt. **7**, 8757 (1995).
4. C.J. Lambert, R. Raimondi, J. Phys. Cond. Matt. **10**, 901 (1998).
5. Y. Imry, *Introduction to Mesoscopic Physics* (Oxford University Press, INC., Oxford, 1997), Chap. 7.
6. G.E. Blonder, M. Tinkham, T.M. Klapwijk, Phys. Rev. B **25**, 4515 (1982); G.E. Blonder, M. Tinkham, Phys. Rev. B **27**, 112 (1983).
7. C.J. Lambert, J. Phys. Cond. Matt. **3**, 6579 (1991).
8. Y. Takane, H. Ebisawa, J. Phys. Soc. Jpn **60**, 3130 (1991); **61**, 1685 (1992); **61**, 2858 (1992).
9. C.W.J. Beenakker, Phys. Rev. B **46**, 12841 (1992); Rev. Mod. Phys. **69**, 731 (1997); in *Mesoscopic Quantum Physics*, edited by E. Akkermans, G. Montambaux, J.-L. Pichard (North-Holland, Amsterdam, 1995).
10. Y. Takagaki, Phys. Rev. B **57**, 4009 (1998); Y. Takagaki, H. Takayanagi, Phys. Rev. B **53**, 14530 (1996); Y. Takagaki, K. Ploog, Phys. Rev. B **51**, 7017 (1995).

11. N.A. Mortensen, K. Flensberg, A.-P. Jauho, Phys. Rev. B **59**, 10176 (1999).
12. A.F. Andreev, Zh. Eksp. Teor. Fiz. **46**, 1823 (1964) [Sov. Phys. JETP **19**, 1228 (1964)]; **51**, 1510 (1966) [**24**, 1019 (1967)].
13. A.F. Morpurgo, B.J. van Wees, T.M. Klapwijk, Phys. Rev. Lett. **79**, 4010 (1997).
14. C.W.J. Beenakker, H. van Houten, Solid State Phys. **44**, 1 (1991).
15. G. Garcia-Calderon, in *The Physics of Low-Dimensional Semiconductor Structures,* edited by P. Butcher, N.H. March, M.P. Tosi (Plenum, New York, 1993), p. 267.
16. J.B. Xia, Phys. Rev. B **45** , 3593 (1992).
17. P.S. Deo, A.M. Jayannavar, Phys. Rev. B **50**, 11629 (1994); A.M. Jaynnavar, P.S. Deo, Mod. Phys. Lett. B **8**, 301 (1994).
18. F. Sols, M. Macucci, V. Ravoili, K. Hess, Appl. Phys. Lett. **54**, 350 (1990).
19. B.Y. Gu, Phys. Rev. B **51**, 16840 (1995); C. Basu, B.Y. Gu, Physica B **215**, 344 (1995); B.Y. Gu, C. Basu, Inter. J. Modern Phys. B **9**, 3085 (1995).
20. P.G. de Gennes, *Superconductivity of Metals and Alloys*, (Benjamin, New York, 1999).
21. H. Tamura, T. Ando, Phys. Rev. **44**, 1792 (1991).
22. S. Chaudhuri, S. Bandyopadhyyay, J. Appl. Phys. **71**, 3027 (1992).
23. J.E. Avron, A. Raveh, B. Zur, Rev. Mod. Phys. **60**, 873 (1988).
24. H.J. Fink, A. López, R. Maynard, Phys. Rev. B **26**, 5237 (1982).
25. J.R. Shi, B.Y. Gu, Phys. Rev. B **55**, 4703 (1997).